

Contents lists available at [SciVerse ScienceDirect](#)

Chemical Physics Letters

journal homepage: www.elsevier.com/locate/cplett

Room-temperature ferromagnetism observed in C-/N-/O-implanted MgO single crystals

Qiang Li^a, Bonian Ye^b, Yingping Hao^b, Jiandang Liu^a, Jie Zhang^a, Lijuan Zhang^a, Wei Kong^a, Huimin Weng^a, Bangjiao Ye^{a,*}^a Department of Modern Physics, University of Science and Technology of China, Hefei 230026, People's Republic of China^b Key Laboratory of Nuclear Analysis Techniques, Shanghai Institute of Applied Physics, Chinese Academy of Sciences, Shanghai 201800, People's Republic of China

ARTICLE INFO

Article history:

Received 13 October 2012

In final form 22 November 2012

Available online xxxxx

ABSTRACT

MgO single crystals were implanted with 70 keV C/N/O ions at room temperature with respective doses of 2×10^{16} and 2×10^{17} ions/cm². All samples with high-dose implantation showed room temperature hysteresis in magnetization loops. Magnetization and slow positron annihilation measurements confirmed that room temperature ferromagnetism in O-implanted samples was attributed to the presence of Mg vacancies. Furthermore, the introduction of C or N played more effective role in ferromagnetic performance than Mg vacancies. Moreover, the magnetic moment possibly occurred from the localized wave function of unpaired electrons and the exchange interaction formed a long-range magnetic order.

© 2012 Elsevier B.V. All rights reserved.

1. Introduction

In recent years, diluted magnetic semiconductors (DMSs) have received increasing interests from scientists due to their spintronics application potential. Room temperature ferromagnetism (RTFM) is observed in transition-metal (TM) doped semiconductors [1–5], which is generally attributed to the presence of transition metal. However, the initial idea was challenged by the ferromagnetism discovery in thin films of undoped HfO₂, in which the expected defects or oxygen vacancies could be the source of ferromagnetism [6]. Recently, defect induced magnetism (DIM) has been observed in series of nanoparticles or films of metallic oxides [7,8]. The magnetic moment origin is attributed to the existence of oxygen vacancies. Subsequent studies on MgO material demonstrated that cation vacancies at sample surfaces are responsible for RTFM [9–12]. For instance, Kumar et al. observed that magnetic moments were dependent on the size of nanoparticles that are relevant to the concentration of Mg vacancies [10]. A series of studies on N-doped MgO proved that localized magnetic moments exist around the N impurity [13–17]. Moreover, ferromagnetic correlations between the two nitrogen impurities have been calculated [15]. However, inconsistencies from previous experiments have been reflected in some theories as they presented opposite views. Wu et al. demonstrated that the C or N ion performance in MgO easily exhibited stable diamagnetism after pairing [18]. Meanwhile, one has to acknowledge the fact that contribution of ferromagnetic impurities in most studies is difficult

to exclude from the total signal observed. Measured impurities are necessary in this research field, which has been carefully presented in a recent study [19].

The nature of ferromagnetism in MgO samples remains unclear. Few experiments on N-doped MgO and C-doped ZnO have been reported thus far [20–22]. However, MgO-based FM via C-doping has not been experimentally investigated. In the current Letter, the experimental results on the magnetic properties of C-/N-/O-implanted MgO single crystals are reported. Positron annihilation spectroscopy was used to characterize the defects and vacancies in the implanted samples. The discovery of RTFM may provide a valuable reference for further theories on DIM.

2. Experiment

MgO single-crystal wafers, prepared through arc melting and packaged in a vacuum bag prior to use, were obtained commercially from the Chinese Academy of Sciences (Shanghai). Inductively coupled plasma emission spectroscopy (ICP-ES) was used to detect ferromagnetic impurities in raw wafers [23]. The results are shown in Table 1.

The ICP-ES analysis showed traces of Fe, Co, Ni, Mn, Cr, and Ca impurities. Ferromagnetic impurities in wafers were demonstrated as small because the content was normally less than 10 ppm for each element. XRF measurement only showed Ca impurity peak and ICP-ES showed that Ca ion content was 1.16 mg/g. Ca ions are presumably diamagnetic and do not contribute to the paramagnetic response [19].

Injection experiment was completed using a 100 keV Electro-magnetic Isotope Separator at the Shanghai Institute of Applied

* Corresponding author.

E-mail address: bjye@ustc.edu.cn (B. Ye).

Table 1
Results of the ICP-ES analysis.

	Fe	Co	Ni	Mn	Cr
Concentrations($\mu\text{g/g}$)	15.20	1.25	12.34	10.67	16.02

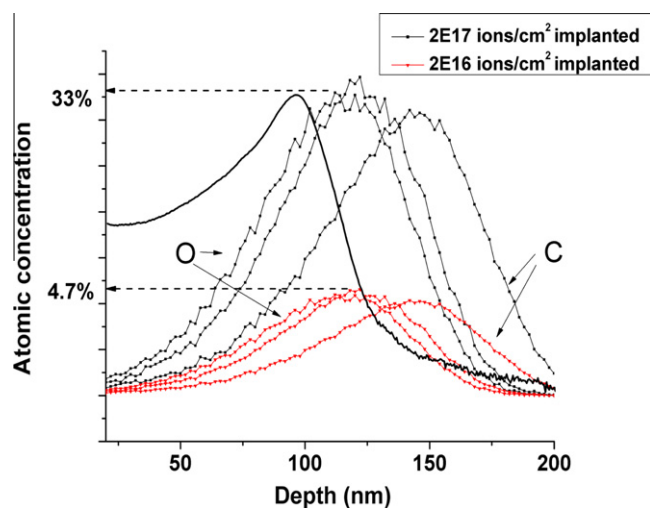


Figure 1. Depth profiles of injected ions simulated with SRIM. The solid line represents the depth profile of C ions in a high dose sample analyzed by SIMS.

Physics (SIAP). C, N, and O-ions at 70 keV were implanted into the polished surface of different MgO crystals with the dose was divided into $2 \times 10^{16}/\text{cm}^2$ and $2 \times 10^{17}/\text{cm}^2$, respectively. The processes maintained a base pressure of 2.2×10^{-4} Pa and a nearby controlled room temperature. Wafers were deeply colored after implantation. The depth profiles of injected ions are shown in Figure 1. Average implantation depth by the Stopping and Ranges of Ions in Matter (SRIM) simulation was approximately 120 nm for O and N, and approximately 150 nm for C. Solid line represents the depth profile of C ions in high dose sample analyzed using Secondary Ion Mass Spectrometry (SIMS). The real implantation depth of C ions was approximately 100 nm. The atomic concentration of implanted ions was estimated using the density of samples which gave impurity peak concentrations of 33% and 4.7% for the higher and lower implantation dose, respectively. All the samples were cut into $6 \times 8 \times 0.5$ mm, and then carefully decontaminated with ultrasonic acetone. Room-temperature magnetic properties were obtained using the Vibrating Sample Magnetometer (VSM) with an accuracy of 10^{-7} emu. Measurements were carefully conducted to avoid contact with the magnetic apparatus to ensure the exclusion of magnetic impurities influences. The structure and defects of the samples were demonstrated by X-ray diffraction spectroscopy and slow positron annihilation measurements.

3. Results and discussions

Figure 2 shows the VSM results of all samples. All magnetic curves were treated to subtract background signals influences, which include diamagnetic substrate, measurement of straws,

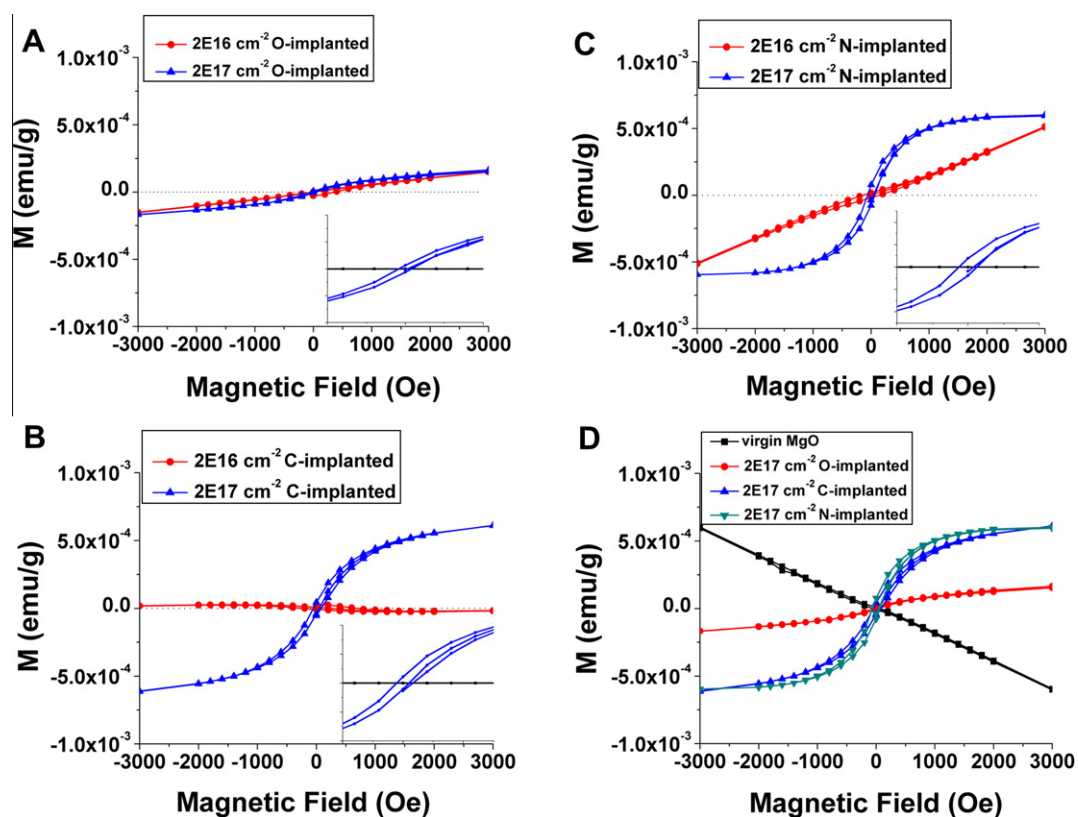


Figure 2. The magnetization versus magnetic field measured at 300 K for (a) O-, (b) C-, (c) N- implanted MgO with implantation dose of 2×10^{16} and 2×10^{17} ions cm^{-2} . Raw curve of virgin MgO is shown in pattern (d). The insets show apparent low field hysteresis loops for the samples implanted dose of 2×10^{17} ions cm^{-2} . The diamagnetic background has been subtracted.

and possible influence of impurities in wafers. Ferromagnetism at room temperature could be observed among all samples with $2 \times 10^{17}/\text{cm}^2$ implantation dose.

O-implantation does not introduce any impurities into MgO. The well-defined hysteresis loop in Figure 2a indicates that the observed RTFM is attributed to the implantation-induced defects. For the C-group in Figure 2b, the lower-dose sample did not exhibit significant change compared with virgin wafer. However, the higher-dose sample showed an obvious hysteresis, with saturation magnetization of approximately 5×10^{-4} emu, which is four times larger than the O-implanted higher-dose sample. Coercivity field was approximately 50 Oe. Figure 1c shows that the N implanted lower-dose sample showed a significant change in magnetism, but not a clearly identifiable coercive field. The higher-dose sample showed a ferromagnetism change, with saturation magnetization almost equal to the C-implanted sample (Figure 1d). Coercive field was approximately 60 Oe. Compared with O-implanted sample, there is a remarkable change in both the saturation magnetization and coercivity for these samples implanted with C and N ions, even though the implantation dose is almost the same. This is a strong indication that defects alone is not the only parameter that influences the magnetic characteristics of the MgO:C and MgO:N. It's believed that the presence of C or N element also play a significant role in RTFM origination in C- or N-doped samples.

Figure 3 displays the XRD measurements of implantation-induced lattice distortion. All samples showed only MgO(200) peak corresponding to cubic rock salt structure and no any extra second-phase diffraction peaks were formed after implantation (2θ from 20 to 80). The full width at half-maximum (FWHM) values for the virgin sample was 0.18° and no significant changes were observed in lower-dose implanted samples. However, a clear broad feature appears at the left side of the MgO(200) peak for all the higher-dose implanted samples. The FWHM values for the C- and N-implanted samples were 1.24° and 1.23° , respectively, indicating the lattice disorder due to the implantation induced defects. For the O-implanted sample, apparent two peaks were observed at the (200) plane which give the FWHM were 1.33° (left peak) and 0.25° (right peak), respectively. This indicates that the crystal in the O-implanted layers becomes more imperfect due to lattice distortion. Peak broadening for higher-dose samples after O-implantation may be attributed to the induced Mg related vacancies or clusters. Meanwhile, lattice expansion induced by interstitial atoms was also a reason for the peak broadening and left movement in C or N implanted MgO. For C-implanted sample, the substitution of O by implanted C will expand the lattice [21]. Thus, this Letter assumed that the implanted defects are mainly lattice expansion or cation vacancies/clusters.

Slow positron annihilation spectroscopy, an effective tool for detecting vacancy-type defects in materials, was also utilized to determine the nature of the induced defects in C- and O-implanted higher-dose samples. The measurements were carried out using the mono-energetic positron beam, and positron energy varied from 0.25 to 15 keV. Doppler broadening of annihilation radiation was measured by a Ge detector. The motion of electron-positron pair prior to annihilation caused Doppler broadening in the 511 keV annihilation line and can be characterized by the line-shaped parameter S [24], which is defined as the ratio of counts in the central region of 511 keV to the total number of counts in the peak. Therefore, an increase in the S parameter indicates the introduction of vacancy defects. Figure 4 displays the S parameter as a function of incident positron energy for virgin, O-, and C-implanted higher-dose MgO. The corresponding mean implantation depth is shown in the top axes. The positrons with an energy range from 0.25 to 1.5 keV annihilate at the surface of the samples. The largest S-parameters in this layer were normally due to the formation and annihilation of positronium atoms at the surface

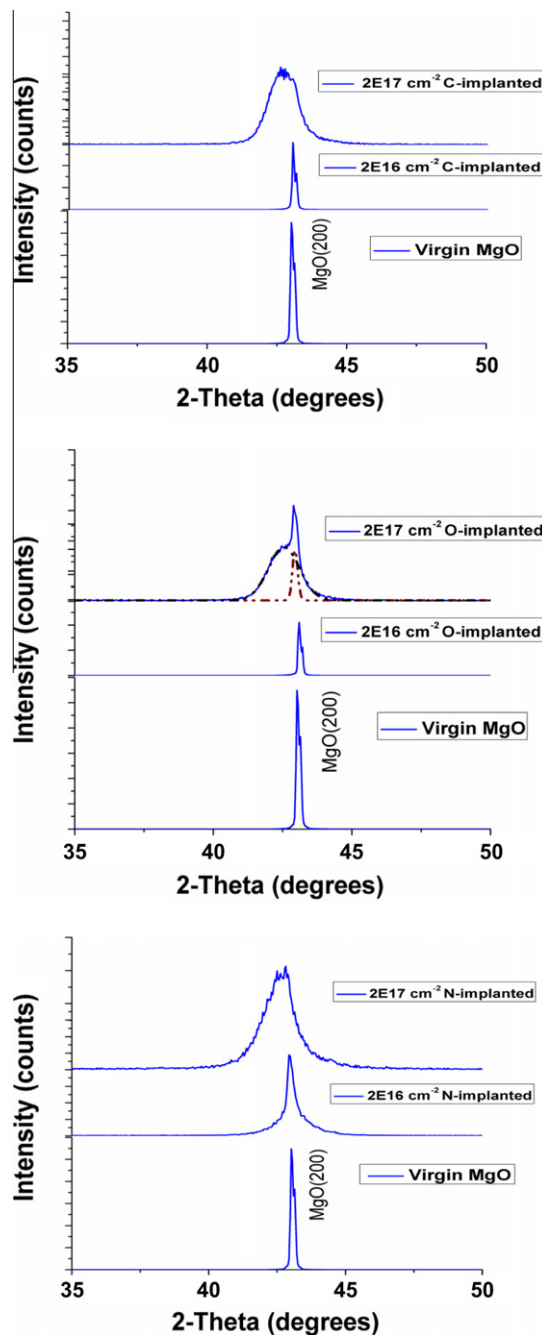


Figure 3. XRD patterns of (up) C-implanted samples, (middle) O-implanted samples, (bottom) N-implanted samples. For each graph, the top pattern corresponds to the higher implantation dose.

of materials [25]. The energy range between 1.5 and 7.5 keV is regarded as the feature of the ion-implanted layer. While the incident energy above 7.5 keV, positrons annihilate mainly in the MgO substrate, leading to over-lapping of the three plots. The increase of S-parameters in the injection layer clearly showed the emergence of induced defects. Figure 5 displays the plots of W values as a function of S value for the O- and C-implanted samples. The W parameter was defined as a fraction of counts in the wing area of the 511 keV peak [26]. Each defect type exhibits its own specific S and W parameter. Thus, the linear relationship between S–W indicates that the two samples contain the same vacancy defects [27]. Cation vacancies are dominant positron trapping defects in materials. The significant increase of S-parameter in both samples definitely showed that the induced defects are mainly

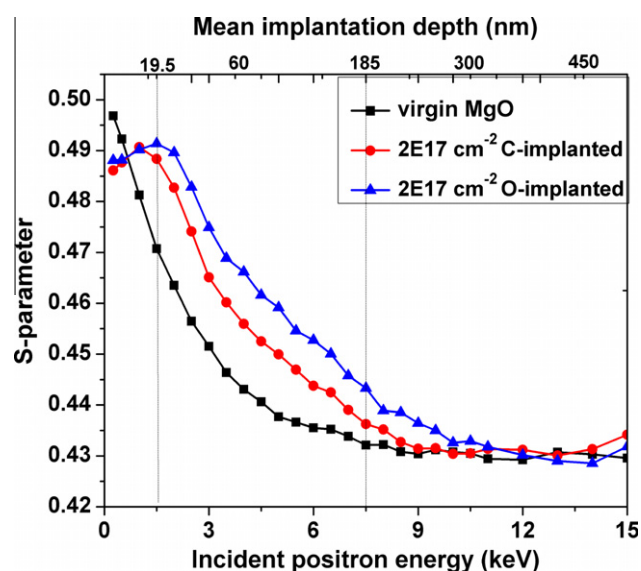


Figure 4. S-E curves measured for virgin, O-, and C-implanted MgO with implantation dose of 2×10^{17} ions cm^{-2} . The lines are drawn to guide the eye.

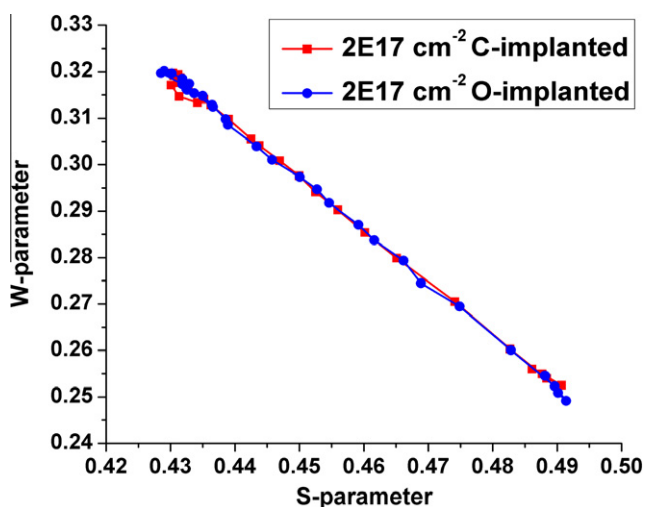


Figure 5. The dependence of S and W parameters.

Mg related vacancies. Moreover, the observed RTFM originated in the electronic status around Mg vacancies due to the spin polarization of 2p electrons of the oxygen atoms surrounding the Mg vacancies, in view of suggested theories [28]. The S-parameter increase observed in the O-implanted sample was higher than the C-implanted sample, clearly indicating that the concentration of Mg vacancies caused by O-implantation was greater than that of C-implantation. Given the significant distinction of saturation magnetization, Mg vacancies were not eligible for the main origin of ferromagnetism in the C implanted sample. It's believed that Most of the observed RTFM are attributed to the presence of the C-element. The introduction of C or N was also proven to play more effective role in ferromagnetic performance than Mg vacancies.

As a wide band-gap material, the MgO samples are highly resistive. Experiments show that the carrier concentration in samples is too low to be detected by Hall Effect, which suggests that FM does not depend upon the presence of a significant carrier concentration. Actually, injection-induced holes (unpaired electrons) are the source of localized moment in insulating MgO. Ferromagnetic coupling can be interpreted as the exchange interaction in the

localized wave function. The d0 ferromagnetism in MgO can probably be understood using the phenomenological bound magnetic polaron model [29]. Defects or impurities that have a triplet ground state or low-lying triplet excited state may form an impurity band by themselves, taking over the 'magnetic polaron'. Thus, ferromagnetism strongly depends on the concentration of impurities.

All ferromagnetic signals assumingly attribute to the presence of C or N ions. In addition, the saturation magnetization was estimated by only 0.027 μB per C or N, which was lesser than the theoretically predicted value of 2 $\mu\text{B}/\text{C}$ and even the experimentally reported value of 0.06 $\mu\text{B}/\text{C}$ in ZnO [13,21]. However, it is a common phenomenon that the experimental results of magnetic moment are lesser than the theoretical values. Moreover, the average moment will be decreased when the doping concentration increases. Excessive doping probably inhibits part of the performance of magnetism, resulting in an average magnetic moment decrease. For higher-dose samples, several injected impurities too close to each other possibly lead to the formation of antiferromagnetic pairs [30]. Another fact is that a large number of atoms, which are located in low concentrated regions as shown in Figure 1, do not contribute to the observed RTFM. It could be seen that the high-dose samples contain paramagnetic component because of nearly isolated impurity ions. Lower-dose samples without ferromagnetism can be interpreted as the peak concentration at 4.7%; hence, the critical value which visible ferromagnetism required could not still be achieved. The paramagnetic performance of lower-dose samples in Figure 2a and c was due to isolated moments formation.

4. Conclusion

In summary, apparent RTFM was observed in C-, N-, and O-implanted higher-dose MgO samples. The magnetic moment origin and the ferromagnetism in O-implanted MgO are due to the implantation-induced Mg vacancies. C and N impurities definitely contribute to the observed RTFM in C/N-implanted samples, which are even more effective than Mg vacancies. Localized magnetic moment as the key factor of ferromagnetic coupling has also been discussed.

Acknowledgments

This work is supported by the State Key Program of National Natural Science of China (Grant No. 10835006) and 211 project of Ministry of Education of China. The authors would like to thank Ph.D. Xue for the measurement of slow positron annihilation.

References

- [1] Nguyen Hoa Hong, Joe Sakai, W. Prellier, Awatef Hassini, Antoine Ruyter, François Gervais, Phys. Rev. B 70 (2004) 195204.
- [2] Y.W. Heo et al., Appl. Phys. Lett. 84 (2004) 2292.
- [3] M. Bolduc, C. Awo-Affouda, A. Stollenwerk, M.B. Huang, F.G. Ramos, G. Agnello, V.P. LaBella, Phys. Rev. B 71 (2005) 033302.
- [4] R.P. Borges, J.V. Pinto, R.C. da Silva, A.P. Goncalves, M.M. Cruz, M. Godinho, J. Magn. Mater. 316 (2007) e191.
- [5] Zhongquan Mao, Zhenhui He, Dihua Chen, W.Y. Cheung, S.P. Wong, Solid State Commun. 142 (2007) 329.
- [6] M. Venkatesan, C.B. Fitzgerald, J.M.D. Coey, Nature (London) 430 (2004) 630.
- [7] A. Sundaresan, R. Bhargavi, N. Rangarajan, U. Siddesh, C.N.R. Rao, Phys. Rev. B 74 (2006) 161306(R).
- [8] Nguyen Hoa Hong, Joe Sakai, Nathalie Poirot, Virginie Brizé, Phys. Rev. B 73 (2006) 132404.
- [9] Jifan Hu, Zhongli Zhang, Ming Zhao, Hongwei Qin, Minhua Jiang, Appl. Phys. Lett. 93 (2008) 192503.
- [10] Nitesh Kumar, D. Sanyal, A. Sundaresan, Chem. Phys. Lett. 477 (2009).
- [11] C. Moyses Araujo et al., Appl. Phys. Lett. 96 (2010) 232505.
- [12] Mukes Kapilashrami, Jun Xu, K.V. Rao, Lyuba Belova1, Elin Carlegrim, Mats Fahlman, J. Phys.: Condens. Matter 22 (2010) 345004.

- [13] A. Droghetti, C.D. Pemmaraju, S. Sanvito, *Phys. Rev. B* 78 (2008) 140404(R).
- [14] A. Droghetti, S. Sanvito, *Appl. Phys. Lett.* 94 (2009) 252505.
- [15] Bo Gu, Nejat Bulut, Timothy Ziman, Sadamichi Maekawa, *Phys. Rev. B* 79 (2009) 024407.
- [16] Phivos Mavropoulos, Marjana Ležaić, Stefan Blügel, *Phys. Rev. B* 80 (2009) 184403.
- [17] Matteo Pesci, Federico Gallino, Cristiana Di Valentin, Gianfranco Pacchioni, *J. Phys. Chem. C* 114 (2010) 1350.
- [18] Wu Hua, Alessandro Stroppa, Sung Sakong, Silvia Picozzi, Matthias Scheffler, Peter Kratzer, *Phys. Rev. Lett.* 105 (2010) 267203.
- [19] M. Khalid, A. Setzer, M. Ziese, P. Esquinazi, D. Spemann, A. Pöpl, E. Goering, *Phys. Rev. B* 81 (2010) 214414.
- [20] Liu Chun-Ming, Hai-Quan Gu, Xia Xiang, Yan Zhang, Yong Jiang, Men Chen, Xiao-Tao Zu, *Chin. Phys. B* 20 (4) (2011) 047505.
- [21] Shengqiang Zhou et al., *Appl. Phys. Lett.* 93 (2008) 232507.
- [22] H. Pan et al., *Phys. Rev. Lett.* 99 (2007) 127201.
- [23] C.J. Pickford, R.M. Brown, *Spectrochim. Acta Part B: At. Spectrosc.* 41 (1–2) (1986) 183.
- [24] M. Khalid et al., *Phys. Rev. B* 80 (2009) 035331.
- [25] B.Y. Zhang et al., *Appl. Phys. Lett.* 99 (2011) 182503.
- [26] Z.Q. Chen, T. Sekiguchi, X.L. Yuan, M. Maekawa, A. Kawasuso, *J. Phys.: Condens. Matter* 16 (2004) S293.
- [27] L. Liskay, C. Corbel, L. Baroux, *Appl. Phys. Lett.* 64 (1994) 1380.
- [28] C. Martínez-Boubeta et al., *Phys. Rev. B* 82 (2010) 024405.
- [29] J.M.D. Coey, M. Venkatesan, C.B. Fitzgerald, *Nat. Mater.* 4 (2005) 173.
- [30] Haowei Peng, H.J. Xiang, Su-Huai Wei, Shu-Shen Li, Jian-Bai Xia, Jingbo Li, *Phys. Rev. Lett.* 102 (2009) 017201.